



Cite this: RSC Adv., 2019, 9, 5100

Received 24th December 2018  
 Accepted 24th January 2019

DOI: 10.1039/c8ra10538c  
[rsc.li/rsc-advances](http://rsc.li/rsc-advances)

## Fabrication of Ag/AgBr/Ag<sub>3</sub>VO<sub>4</sub> composites with high visible light photocatalytic performance

Wenxue Li,<sup>a</sup> Qianlin Chen,<sup>ID \*ab</sup> Xianyu Lei<sup>a</sup> and Shang Gong<sup>a</sup>

Herein, Ag/AgBr/Ag<sub>3</sub>VO<sub>4</sub> composites were synthesized by a simple continuous precipitation method. The obtained composites were characterized by X-ray diffraction (XRD), scanning electron microscopy (SEM), energy dispersive spectrometry (EDS), X-ray photoelectron spectroscopy (XPS), UV-vis diffuse reflectance spectroscopy and photoluminescence spectroscopy (PL). Photocatalytic performance of the composites was assessed by the degradation of methyl orange (MO) and tetracycline hydrochloride (TC) under visible light, and the effects of different nominal mass ratios of AgBr and Ag<sub>3</sub>VO<sub>4</sub> on the photocatalytic activity were investigated. The results showed that after 20 min of visible light irradiation ( $\lambda > 420$  nm), the removal rate of MO in the presence of a 5 : 1 sample reached 98.6%. The EIS and photocurrent results demonstrated that the enhancement of the visible light photocatalytic activity was attributed to the efficient electron–hole pair separation. In addition, the scavenging reactions conducted *via* the addition of different scavengers confirmed that  $\text{h}^+$  and  $\cdot\text{O}_2^-$  were the main active species in the reaction. The present study offers potential for the degradation of contaminants.

## 1. Introduction

With the gradual development of industry and technology, serious environmental pollution and the scarcity of clean energy have become the most urgent problems. Various forms of organic wastewater are discharged into the environment every year; this has caused serious pollution to the environment. Moreover, the compound structure of organic pollutants is quite stable in water, difficult to decompose, and resistant to biodegradation.<sup>1–4</sup> Some advanced oxidation processes, such as the Fenton oxidation,<sup>5</sup> photocatalytic oxidation<sup>6</sup> and photo-electro-catalytic technology,<sup>7,8</sup> have been developed to solve the problem of wastewater pollution. Photocatalytic oxidation has the advantages of mild reaction conditions, no secondary contamination, and low energy consumption in the reaction process and thus has become one of the best green environmental protection technologies to be developed.<sup>9–11</sup> To date, the most commonly used photocatalyst is TiO<sub>2</sub> that has excellent chemical stability and is abundant, non-toxic, and low-cost.<sup>12,13</sup> However, TiO<sub>2</sub> is a photocatalyst with a wide band gap (3.2 eV), and its low solar energy utilization and quantum yield limit its practical application.<sup>14–16</sup> Researchers have tried to develop a variety of photocatalytic materials with effective visible light responses, which has already been a key problem in the field of photocatalysis. In the past few years, many studies have been conducted on

silver-based photocatalysts, including Ag<sub>2</sub>O,<sup>17</sup> Ag<sub>3</sub>PO<sub>4</sub>,<sup>18</sup> Ag<sub>2</sub>CO<sub>3</sub>,<sup>19</sup> AgX (X = Cl, Br, I),<sup>20</sup> and Ag<sub>6</sub>Si<sub>2</sub>O<sub>7</sub>,<sup>21,22</sup> with excellent properties in the degradation of organic pollutants.

AgBr is a traditional photosensitive material whose properties of light decomposition greatly limit its application as a photocatalyst.<sup>23,24</sup> Studies have shown that AgBr can reduce its surface component Ag<sup>+</sup> to Ag<sup>0</sup> under illumination to form Ag/AgBr, and the photocatalytic activity of Ag/AgBr is improved because Ag<sup>0</sup> exhibits a high efficiency plasmon resonance effect (SPR) in the visible region.<sup>25</sup> Since the electron–hole pairs of AgBr rapidly combine, AgBr is generally mixed with other materials to improve its photocatalytic performance. Chen *et al.*<sup>26</sup> synthesized a AgBr@rGO composite by coating AgBr on graphene nanosheets *via* a precipitation method; this increased the separation rate of the photogenerated charges. Upon further loading AgBr onto the graphene hydrogel to form a 3D network structure with good adsorption performance, bisphenol A rapidly degraded under the synergistic effect of adsorption and photocatalytic degradation. Lin *et al.*<sup>27</sup> studied the decoration of nano Ag@AgBr particles on flower-like Bi<sub>2</sub>WO<sub>6</sub> using an oil-in-water self-assembly method to form Ag@AgBr/Bi<sub>2</sub>WO<sub>6</sub> composites, whose degradation rate for MB was 1.29 times that of Ag@AgBr. In summary, it can be clearly concluded that the AgBr-based composite materials show better photocatalytic activity in the degradation of organic pollutants.

Ever since Konta *et al.*<sup>28</sup> have conducted a pioneering study on Ag<sub>3</sub>VO<sub>4</sub> and found that Ag<sub>3</sub>VO<sub>4</sub> can split H<sub>2</sub>O into O<sub>2</sub> and H<sub>2</sub>, the narrow band gap monoclinic scheelite Ag<sub>3</sub>VO<sub>4</sub> ( $\sim$ 2 eV) has attracted wide attention of researchers. Due to its special band structure, the electron–hole recombination rate of pure Ag<sub>3</sub>VO<sub>4</sub>

<sup>a</sup>School of Chemistry and Chemical Engineering, Guizhou University, Guiyang, 550025, China. E-mail: cql1018@163.com

<sup>b</sup>Institute of Advanced Technology, Guizhou University, Guiyang, 550025, China



is higher.<sup>29</sup> Many researchers have further modified its photocatalytic properties by combining it with a large number of materials such as  $\text{WO}_3$ ,<sup>30</sup>  $\text{BiVO}_4$ ,<sup>31</sup>  $\text{ZnO}$ ,<sup>32</sup>  $\text{g-C}_3\text{N}_4$ ,<sup>33</sup> and  $\text{BiOBr}$ .<sup>34</sup> In general, the construction of a heterojunction photocatalyst is a method that can effectively improve the performance of a single photocatalyst. Zhu *et al.*<sup>35</sup> have reported the initial combination of  $\text{Ag}_3\text{VO}_4$  and  $\text{AgBr}$  materials; however, investigation of the ideal ratio of each material is still worth further exploration; in addition, the preparation of a composite photocatalyst of the system by a continuous precipitation method and the development of the composite  $\text{Ag}/\text{AgBr}/\text{Ag}_3\text{VO}_4$  for the degradation of MO and TC have not been reported to date.

In this study, a series of  $\text{Ag}/\text{AgBr}/\text{Ag}_3\text{VO}_4$  photocatalysts with different  $\text{AgBr}$  masses were synthesized by a simple continuous precipitation method. The visible light catalytic performance of the photocatalyst in the degradation of MO and TC was investigated. The effects of different active substances during the degradation of MO were also studied by introducing various scavengers into the photocatalytic reaction system. The separation efficiency of electron-hole pairs has been discussed by investigating the electrochemical properties, and the possible mechanism of the photocatalytic processes has been proposed.

## 2. Experimental

### 2.1. Chemicals

Silver nitrate ( $\text{AgNO}_3$ ) was purchased from Sinopharm Chemical Reagent Co., Ltd (Shanghai, China). Potassium bromide (KBr) was purchased from Chengdu Jinshan Chemical Reagent Co., Ltd. Sodium vanadate ( $\text{Na}_3\text{VO}_4$ ) was purchased from Cool Chemistry (Beijing, China). Methyl orange (MO) was purchased from Chengdu Jinshan Chemical Reagent Co., Ltd. Tetracycline hydrochloride (TC) was purchased from Aladdin (Shanghai, China). All reagents were of analytical grade and used without further purification.

### 2.2. Synthesis of the $\text{Ag}/\text{AgBr}/\text{Ag}_3\text{VO}_4$ photocatalyst

A series of  $\text{Ag}/\text{AgBr}/\text{Ag}_3\text{VO}_4$  composites were prepared through a continuous precipitation route. In a typical synthetic procedure, a certain amount of  $\text{AgNO}_3$  (7.6, 6.7, 6.3, 6.1 mmol) was added to 50 mL of deionized water followed by stirring to obtain a uniform clear solution, labeled as solution A. Then, 5.3 mmol of KBr was dissolved in 20 mL of deionized water and marked as solution B. A certain amount of  $\text{Na}_3\text{VO}_4$  (0.76, 0.46, 0.33, 0.25 mmol) was added to another 20 mL of deionized water and labeled as solution C. The solution B was gradually added dropwise to the solution A *via* a dropping funnel under vigorous stirring. After 30 min,  $\text{Ag}^+$ - $\text{AgBr}$  was obtained. Then, solution C was continuously added to the above mentioned mixture in the same manner, and magnetic stirring was further continued for another 4 h to obtain the  $\text{AgBr}/\text{Ag}_3\text{VO}_4$  composites. After this, the mixture solution was reduced under visible light for 20 minutes to produce a portion of  $\text{Ag}^0$ . The final product was obtained by filtration, rinsed three times with deionized water and placed in an oven at 60 °C for 24 h. The nominal mass ratios

of  $\text{AgBr}$  to  $\text{Ag}_3\text{VO}_4$  were 3 : 1, 5 : 1, 7 : 1, and 9 : 1, and the corresponding samples were denoted as S1, S2, S3, S4. In brief, pure  $\text{Ag}/\text{AgBr}$  was prepared by precipitation of 3 mmol  $\text{AgNO}_3$  with 3 mmol KBr followed by photoreduction for 20 minutes.  $\text{Ag}_3\text{VO}_4$  was obtained by precipitation of 6 mmol  $\text{AgNO}_3$  with 2 mmol  $\text{Na}_3\text{VO}_4$ .

### 2.3. Evaluation of the photocatalytic performance

The photocatalytic reactions occurred in a 200 mL reactor at room temperature, and a 300 W Xe lamp (CEL-HXF300) equipped with a 420 nm cut-off filter was used as the light source for the reaction process. Typically, 50 mg photocatalyst was added to 100 mL of MO (10 mg L<sup>-1</sup>) solution (or 50 mg photocatalyst was added to 100 mL of TC (10 mg L<sup>-1</sup>) solution), and the mixture was stirred in the dark for 30 min to ensure an adsorption-desorption balance. Then, the light source was turned on for photocatalysis experiments, and timing was initiated. During the reaction, quantitative samples were obtained at given time intervals under light irradiation. The sample was centrifuged at 10 000 rpm for 5 min to separate the catalyst from the solution. Analysis of the absorbance of the supernatant at each of the abovementioned intervals was performed using a UV-vis spectrophotometer. The role of various active species in the photocatalytic system was investigated by adding different active species capture agents, including 0.2 g ammonium oxalate (AO), 3 mL isopropanol (IPA) and 8 mg benzoquinone (BQ), to the solution.

### 2.4. Characterization of the as-prepared samples

To discriminate the phase composition and purity of the materials, X-ray diffraction (XRD) analysis of the samples was conducted using the D8 ADVANCE diffractometer with Cu K $\alpha$  radiation. The morphology and constituent elements of the composites were investigated by scanning electron microscopy (S-4800, accelerating voltage 200 kV) and energy dispersive spectroscopy (EDS) analysis, respectively. The elemental composition and the chemical state of the composites were obtained by X-ray photoelectron spectroscopy (ThermoFisher K-Alpha). UV-vis diffuse reflectance spectra (DRS) were obtained by a spectrophotometer (UV2700, Shimadzu, Japan) in the wavelength range of 200–800 nm. Photoluminescence (PL) spectra of the samples were obtained by the Cary Eclipse fluorescence spectrophotometer (Agilent Technologies). Electrochemical impedance spectroscopy (EIS) was conducted using an electrochemical workstation (CHI760E Shanghai). The Pt electrode, the calomel electrode and the sample electrode played the role of a counter electrode, a reference electrode and a working electrode, respectively, and were placed in a 0.1 M  $\text{Na}_2\text{SO}_4$  electrolyte for measuring the photocurrent.

## 3. Results and discussion

The  $\text{Ag}/\text{AgBr}/\text{Ag}_3\text{VO}_4$  composite was prepared by a simple continuous precipitation method. As shown in Fig. 1, the synthetic route is described as follows: at first, KBr was added dropwise to the  $\text{AgNO}_3$  solution, and  $\text{Br}^-$  in the solution reacted



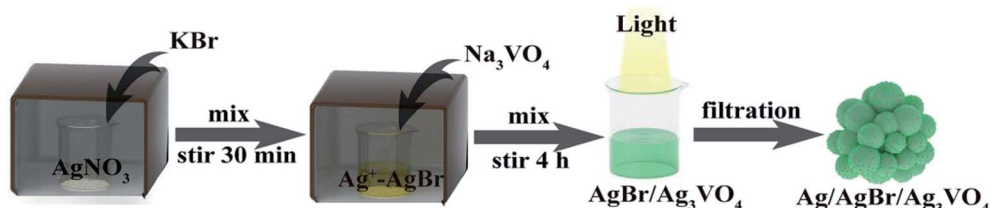


Fig. 1 Schematic of the synthesis route of the  $\text{Ag}/\text{AgBr}/\text{Ag}_3\text{VO}_4$  composites.

with  $\text{Ag}^+$  to form  $\text{AgBr}$ . Then,  $\text{Na}_3\text{VO}_4$  was added to the solution, and  $\text{Ag}^+$  that had been immobilized further reacted with  $\text{VO}_4^{3-}$  to form  $\text{Ag}_3\text{VO}_4$  and covered the surface of  $\text{AgBr}$ . Finally,  $\text{Ag}/\text{AgBr}/\text{Ag}_3\text{VO}_4$  was generated after illumination.

### 3.1. XRD analysis

The XRD spectra of  $\text{Ag}/\text{AgBr}$ ,  $\text{Ag}_3\text{VO}_4$  and  $\text{Ag}/\text{AgBr}/\text{Ag}_3\text{VO}_4$  composites are shown in Fig. 2. The peaks of  $\text{Ag}/\text{AgBr}$  and  $\text{Ag}_3\text{VO}_4$  well-matched with those of cubic  $\text{AgBr}$  (JCPD no. 06-0438) and monoclinic  $\text{Ag}_3\text{VO}_4$  (JCPDS no. 43-0542), respectively. For  $\text{AgBr}$ , the sharp diffraction peaks at  $30.96^\circ$ ,  $44.35^\circ$  and  $55.04^\circ$  corresponded perfectly to the crystal planes of  $(2\ 0\ 0)$ ,  $(2\ 2\ 0)$  and  $(2\ 2\ 2)$ . This shows that its crystallinity is good and there are no other impurities. For pure  $\text{Ag}_3\text{VO}_4$ , the diffraction peaks at  $30.86^\circ$ ,  $32.33^\circ$  and  $35.07^\circ$  corresponded to the crystal planes of  $(-1\ 2\ 1)$ ,  $(1\ 2\ 1)$  and  $(3\ 0\ 1)$ ; this indicated that the prepared  $\text{Ag}_3\text{VO}_4$  was pure and had no second phase. A fairly weak intensity peak can also be observed in the XRD pattern of  $\text{Ag}/\text{AgBr}/\text{Ag}_3\text{VO}_4$ ; since the intensity of the peak of  $\text{Ag}_3\text{VO}_4$  in the composite is much weaker than that of  $\text{AgBr}$  and their peak positions are relatively close at around  $31^\circ$ , the peak of  $\text{Ag}_3\text{VO}_4$  may be covered by the peak of  $\text{AgBr}$ .<sup>36</sup> As the  $\text{AgBr}$  content increases, the peak of  $\text{Ag}_3\text{VO}_4$  becomes weaker until it is barely visible. The results of XRD suggest that the composites have been successfully prepared by a continuous precipitation method. In addition, the reason why the characteristic diffraction peak of  $\text{Ag}^0$ , which is expected to occur, is not observed in the spectrum may be that the content of  $\text{Ag}^0$  is low.

### 3.2. XPS analysis

To acquire the elemental composition of the composite and the chemical states of the measured elements, sample S2 was selected for X-ray photoelectron spectroscopy (XPS). As shown in Fig. 3, the high-resolution spectrum is composed of  $\text{Ag}$  3d,  $\text{Br}$  3d,  $\text{V}$  2p and  $\text{O}$  1s with no other impurities. Moreover, two peaks with the binding energies of  $368.25\text{ eV}$  and  $374.22\text{ eV}$  were observed in the  $\text{Ag}$  3d spectra (Fig. 3b), which were consistent with  $\text{Ag}$  3d<sub>5/2</sub> and  $\text{Ag}$  3d<sub>3/2</sub> of  $\text{Ag}^+$  for  $\text{AgBr}$  and  $\text{Ag}_3\text{VO}_4$ , respectively, and further confirmed that the  $\text{Ag}$  species mainly existed in the form of  $\text{Ag}^+$ . Moreover, there were two weak peaks at the binding energies of  $369.16\text{ eV}$  and  $375.02\text{ eV}$ , which corresponded to  $\text{Ag}$  3d<sub>5/2</sub> and  $\text{Ag}$  3d<sub>3/2</sub>, indicating that  $\text{Ag}$  also existed in the form of metallic  $\text{Ag}^0$ .<sup>37</sup> The reason for the occurrence of this phenomenon is that under light,  $\text{Ag}^+$  is partially reduced to  $\text{Ag}^0$  and attached to the surface of the composite photocatalyst. Moreover, two distinct peaks at the binding energies of  $68.85\text{ eV}$  and  $69.6\text{ eV}$  were observed in the  $\text{Br}$  3d spectra (Fig. 3c), which were attributed to  $\text{Br}$  3d<sub>5/2</sub> and  $\text{Br}$  3d<sub>3/2</sub> and indicated that  $\text{Br}$  existed as  $\text{Br}^-$ .<sup>38</sup> The peaks of  $\text{V}$  2p<sub>1/2</sub> and  $\text{V}$  2p<sub>3/2</sub> at  $516.85\text{ eV}$  and  $524.35\text{ eV}$  confirmed that  $\text{V}$  existed as  $\text{V}^{5+}$  (ref. 39) (Fig. 3d). The peak of  $\text{O}$  1s (Fig. 3e) at  $530.08\text{ eV}$  corresponded to hydroxyls ( $-\text{OH}$ ), and the other peak at  $531.87\text{ eV}$  confirmed the existence of oxygen in  $\text{Ag}/\text{AgBr}/\text{Ag}_3\text{VO}_4$ . All these results further showed that the composites consisted of  $\text{Ag}/\text{AgBr}$  and  $\text{Ag}_3\text{VO}_4$ .

### 3.3. SEM analysis

The morphologies and composition of  $\text{Ag}_3\text{VO}_4$ ,  $\text{Ag}/\text{AgBr}$ , and  $\text{Ag}/\text{AgBr}/\text{Ag}_3\text{VO}_4$  were investigated by SEM and EDS, respectively

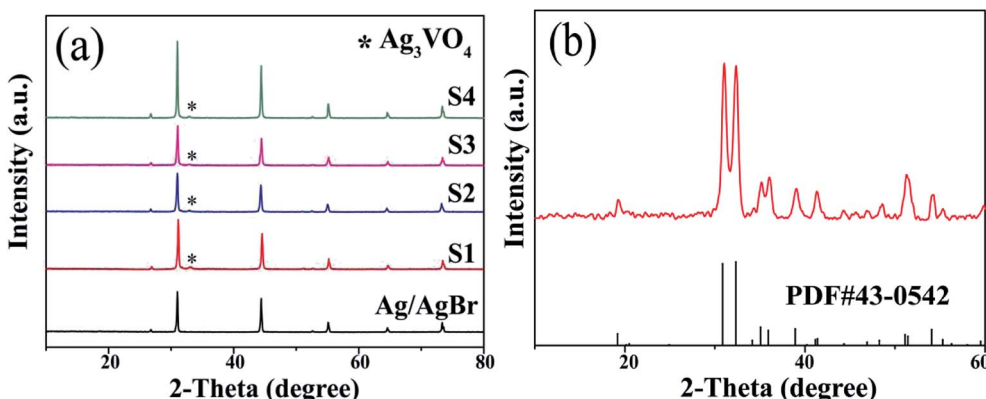


Fig. 2 (a) XRD patterns of  $\text{Ag}/\text{AgBr}$  and  $\text{Ag}/\text{AgBr}/\text{Ag}_3\text{VO}_4$  composites and (b) pure  $\text{Ag}_3\text{VO}_4$ .

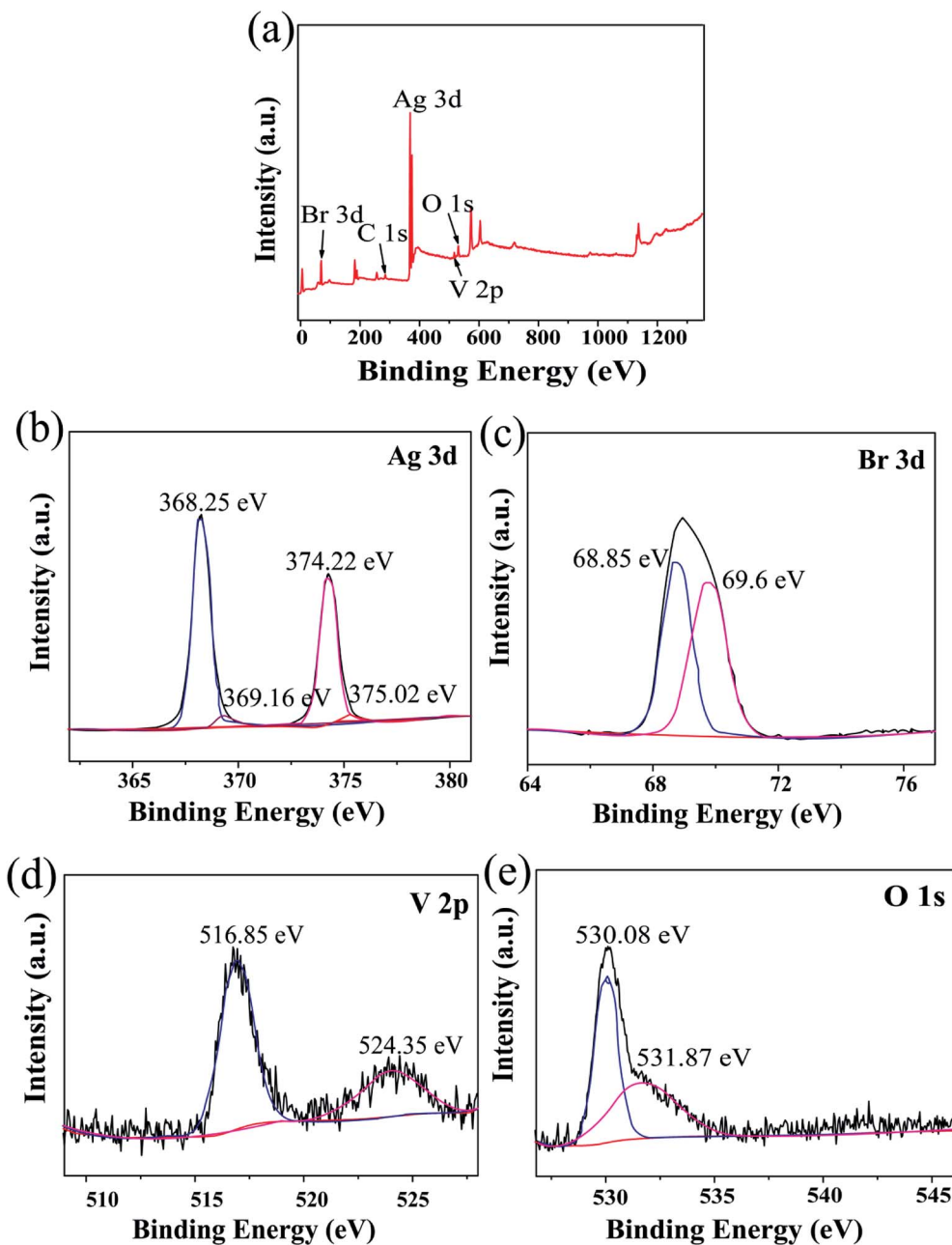


Fig. 3 (a) Survey XPS spectra of the S2 sample; (b, c, d and e) high-resolution XPS data of Ag 3d, Br 3d, V 2p, and O 1s for S2, respectively.

(Fig. 4). As shown in Fig. 4a, fine particles of Ag/AgBr having an average particle diameter of more than 1  $\mu\text{m}$  can be observed. Fig. 4b shows the prepared  $\text{Ag}_3\text{VO}_4$  with nanometer-sized particles. Both Ag/AgBr and  $\text{Ag}_3\text{VO}_4$  prepared by the continuous precipitation method are irregular small particles, and the particle size of  $\text{Ag}_3\text{VO}_4$  is much smaller than that of Ag/AgBr. The composite Ag/AgBr/ $\text{Ag}_3\text{VO}_4$  also exhibited irregular particles, and the surface of the large particles was occupied by many small particles (Fig. 4c). The abundant content of AgBr in the composite material made a significant impact on the formation of its final morphology, and the particle size of the composite was similar to that of AgBr. Moreover, the composite exhibits good dispersibility (Fig. 4d), and the close contact between Ag

and  $\text{Ag}_3\text{VO}_4$  will enhance the transfer and separation of photogenerated charges;<sup>40</sup> one of the advantages of a Ag/AgBr/ $\text{Ag}_3\text{VO}_4$  composite is that it has more active sites, and the photogenerated electron–hole pairs can be rapidly transferred; this is very beneficial to the degradation of MO by the photocatalyst.<sup>41</sup> The EDS spectra of Ag/AgBr and S2 are shown in Fig. 4e and f, respectively. Pure AgBr consisted of Ag and Br elements, whereas the Ag/AgBr/ $\text{Ag}_3\text{VO}_4$  composite material was confirmed to contain Ag, Br, V and O elements. Based on the results of the abovementioned XRD, SEM and EDS data, the preparation of the Ag/AgBr/ $\text{Ag}_3\text{VO}_4$  composite was successfully confirmed.

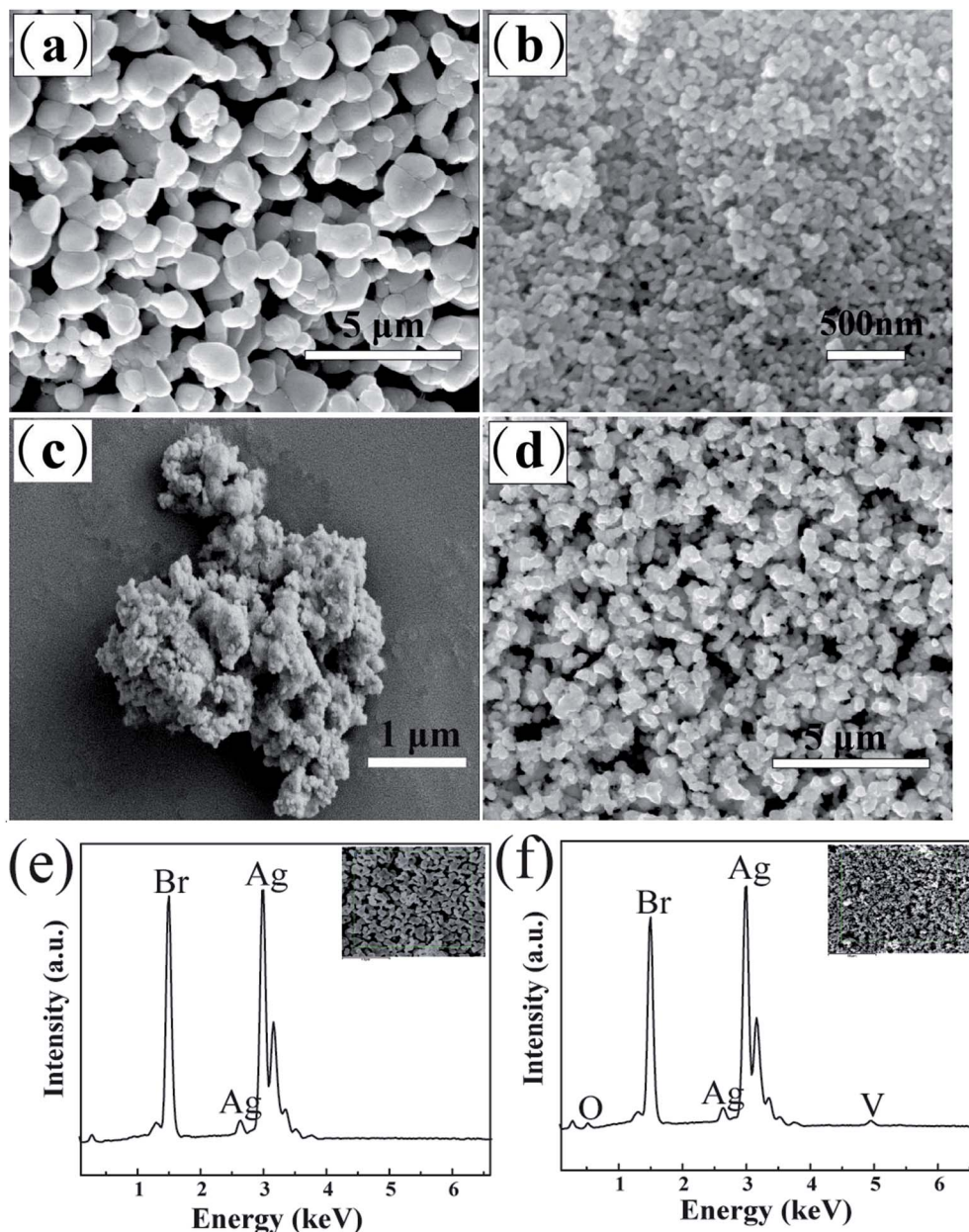


Fig. 4 SEM images of (a) pure Ag/AgBr, (b) pure  $\text{Ag}_3\text{VO}_4$ , and (c and d) S2 sample; (e and f) EDS spectra of pure Ag/AgBr and S2 sample, respectively.

### 3.4. The optical property analysis

The optical properties of the prepared samples were investigated via a UV-vis spectrophotometer. The light absorption characteristic of the composite material can be analyzed from Fig. 5. All samples exhibited absorbance in the visible region, and AgBr caused a significant absorption band in the sample curve due to the surface plasmon resonance effect (SPR) of  $\text{Ag}^0$ , which was derived from the collective oscillation of free electrons.<sup>27,42</sup> With a change in the AgBr content in the composite, the edge absorption band value of the composite appears to increase in a regular way. As the absorption edge value of the sample becomes larger, the response of the sample to visible light is enhanced. The band gap width of the composite materials was obtained by the

equation  $(\alpha h\nu) = A(h\nu - E_g)^{n/2}$ , where  $E_g$ ,  $\nu$ ,  $h$ ,  $A$  and  $\alpha$  are the band gap energy of the semiconductor, light frequency, Planck's constant, a constant value and the absorption coefficient, respectively.<sup>19,34</sup> The relationship between  $(\alpha h\nu)^2$  and  $h\nu$  was obtained as shown in Fig. 5b, and the  $E_g$  value was acquired by estimating the intercept of the tangent of the curve. In this study, the band gap values of Ag/AgBr,  $\text{Ag}_3\text{VO}_4$ , and sample S2 were calculated to be 2.43 eV, 2.01 eV, and 2.64 eV, respectively, which were consistent with the previously reported values.<sup>31,43,44</sup>

### 3.5. Charge separation analysis

In general, PL spectra can be used to detect the separation and recombination rates of photogenerated charges. A lower PL

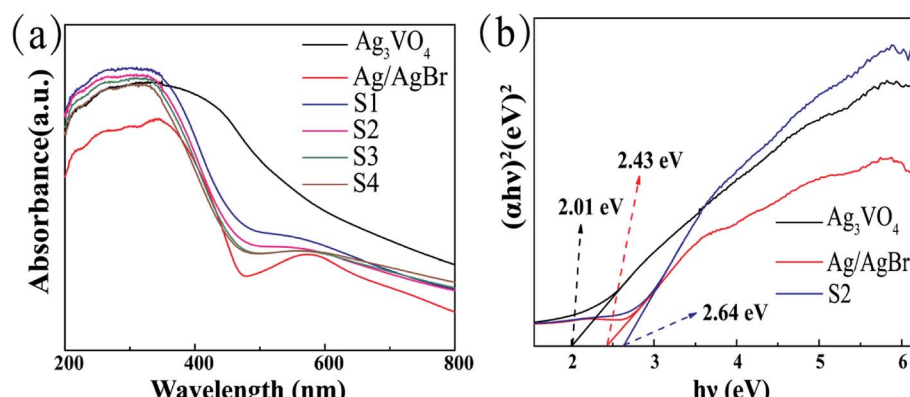


Fig. 5 (a) UV-vis diffuse reflectance spectra of  $\text{Ag}/\text{AgBr}$ ,  $\text{Ag}_3\text{VO}_4$  and  $\text{Ag}/\text{AgBr}/\text{Ag}_3\text{VO}_4$  composites; (b) Tauc plot of  $\text{Ag}/\text{AgBr}$ ,  $\text{Ag}_3\text{VO}_4$  and S2.

intensity means that the photogenerated electron–hole pairs have high separation efficiency and thus produce high photocatalytic activity.<sup>45</sup> The photoluminescence spectra of  $\text{Ag}_3\text{VO}_4$ ,  $\text{Ag}/\text{AgBr}$  and S2 are shown in Fig. 6. It can be found that the intensities of both pure  $\text{Ag}_3\text{VO}_4$  and  $\text{Ag}/\text{AgBr}$  in the plot are higher than those in the curve of the S2 sample at different wavelengths; this indicates the reduction of photogenerated electron–hole pair recombination in sample S2.

To further analyze the separation efficiency of photogenerated electron–hole pairs, the EIS and transient photocurrent responses of the photocatalytic samples were investigated. For the EIS, a small arc radius leads to a low charge transfer resistance.<sup>18</sup> Fig. 7a clearly reveals that the Nyquist plots of S2 are smaller than that of  $\text{Ag}/\text{AgBr}$ ; this indicates that the photogenerated electron–hole transfer efficiency of S2 is high. In the transient photocurrent response of the samples, a change in the light source causes a sudden change in the photocurrent. A high transient photocurrent response is generally indicative of a high separation efficiency of the photogenerated electron–hole pairs. It can be observed that the photocurrent of S2 is stronger than that of  $\text{Ag}/\text{AgBr}$ ; this denotes that S2 has a faster electron–hole separation efficiency (Fig. 7b). This may be due to

the fact that the electron–hole transfer efficiency between interfaces becomes higher after the combination of  $\text{AgBr}$  and  $\text{Ag}_3\text{VO}_4$  into a composite material.

### 3.6. The photocatalytic performance test

To explore the ability of the as-prepared composites to degrade pollutants, the degradation of the common pollutants MO and TC by the composites was studied by the degradation experiments. As shown in Fig. 8a, the negligible self-photolysis of MO under visible light demonstrates that MO has stable chemical properties to light. The adsorption rate in the dark reaction is also low; this indicates that the main cause of MO degradation is visible light irradiation rather than surface adsorption of the photocatalyst. As expected, all the prepared composite photocatalysts have higher photocatalytic activity than  $\text{Ag}/\text{AgBr}$  and  $\text{Ag}_3\text{VO}_4$  with the ranking of S2 > S3 > S4 > S1 >  $\text{Ag}/\text{AgBr}$  >  $\text{Ag}_3\text{VO}_4$ , proving that  $\text{AgBr}$  plays an active role in enhancing the photocatalytic activity.<sup>45</sup> Moreover, as the proportion of  $\text{AgBr}$  in the composites increases, the degradation of MO first increases and then decreases. Particularly, the removal efficiency of all the composite photocatalysts could reach over 90% after 10 min of illumination. S2 exhibited the most excellent photocatalytic activity, and 98.6% of MO was decomposed after 20 min of irradiation. The findings demonstrate that the composite photocatalyst has a shorter degradation time and higher degradation efficiency than the single photocatalyst. The photocatalytic activity of S3 and S4 in the plot is also lower than that of S2; this may be explained by the recombination of photogenerated electrons and holes that suppresses the photocatalytic efficiency. In addition, for the typical colorless antibiotic TC, S2 exhibited superior photocatalytic activity in the degradation of TC (Fig. 8b). Its degradation efficiency reached 77% after 10 minutes. However, after 4 min, the degradation rate of TC became very low, possibly reaching equilibrium rather than complete degradation.<sup>39</sup>

The pseudo first-order plots of MO degradation reactions for different samples are shown in Fig. 8c, which have been obtained by processing the data using a pseudo first-order model whose equation is  $\ln(C_0/C_t) = kt$ .  $C_0$  is the initial concentration of MO before the photoreaction,  $C_t$  is the concentration of MO

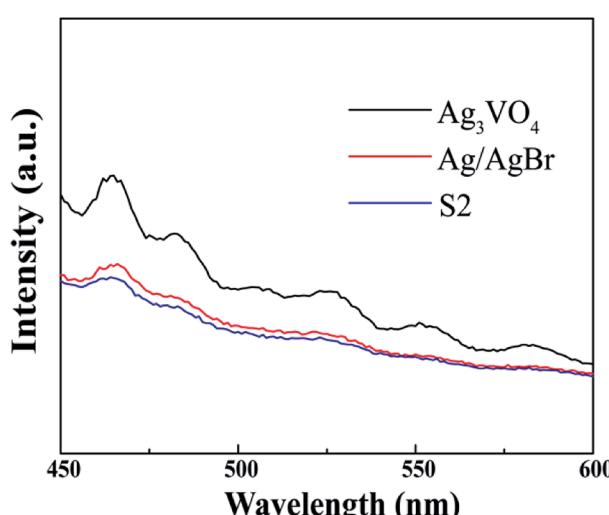


Fig. 6 PL spectra of pure  $\text{Ag}/\text{AgBr}$ ,  $\text{Ag}_3\text{VO}_4$  and S2 sample.



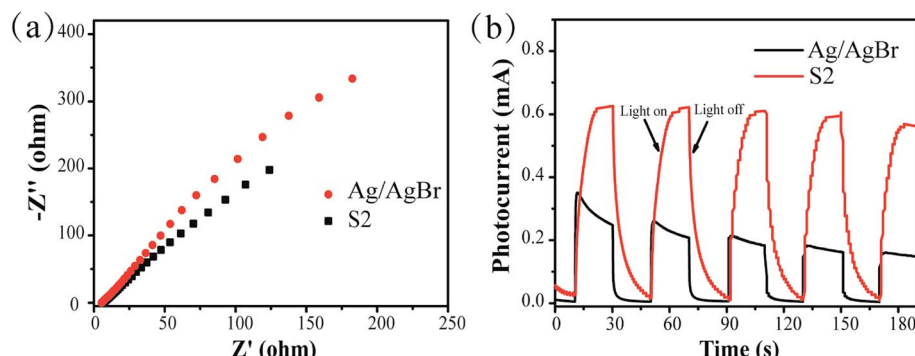


Fig. 7 (a) Electrochemical impedance spectra of Ag/AgBr and S2 photocatalysts and (b) transient photocurrent response of Ag/AgBr and S2.

after the reaction time  $t$ , and  $k$  is the reaction rate constant. The degradation rates of MO were calculated to be  $0.0026\text{ min}^{-1}$ ,  $0.1118\text{ min}^{-1}$ , and  $0.2509\text{ min}^{-1}$  over the  $\text{Ag}_3\text{VO}_4$ , Ag/AgBr, and S2 samples, respectively. The degradation rate of S2 is higher than the degradation rate of a single photocatalyst, which is 2.2 and 96.5 times that of Ag/AgBr and  $\text{Ag}_3\text{VO}_4$ , respectively. This is highly consistent with the results of photocatalytic degradation. These results more accurately demonstrate that the composite

material significantly improves the degradation rate of the pollutants.

The MO solution was taken at a given reaction time, and the change in its TOC content was measured to account for the change of the remaining content of MO in the solution. As shown in Fig. 8d, during the photocatalytic degradation of MO, the TOC gradually decreased to 31% with time. It showed that the composite could effectively remove MO, and MO was mineralized into  $\text{CO}_2$  and  $\text{H}_2\text{O}$ .

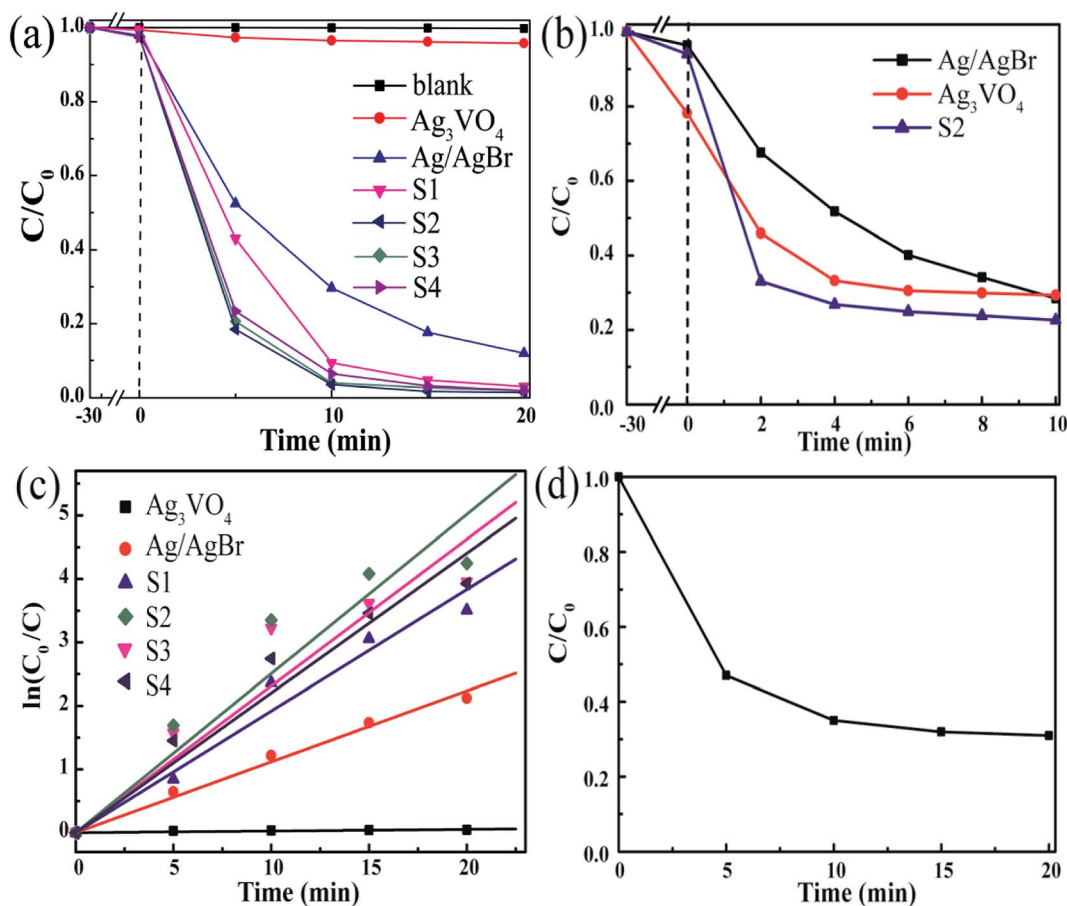


Fig. 8 (a) The photocatalytic degradation of MO via different as-synthesized photocatalysts; (b) the photocatalytic degradation of TC via different as-synthesized photocatalysts; (c) pseudo first-order plot of the photocatalytic degradation of MO via different as-synthesized photocatalysts; (d) change of TOC removal rate of MO in the presence of the S2 sample.

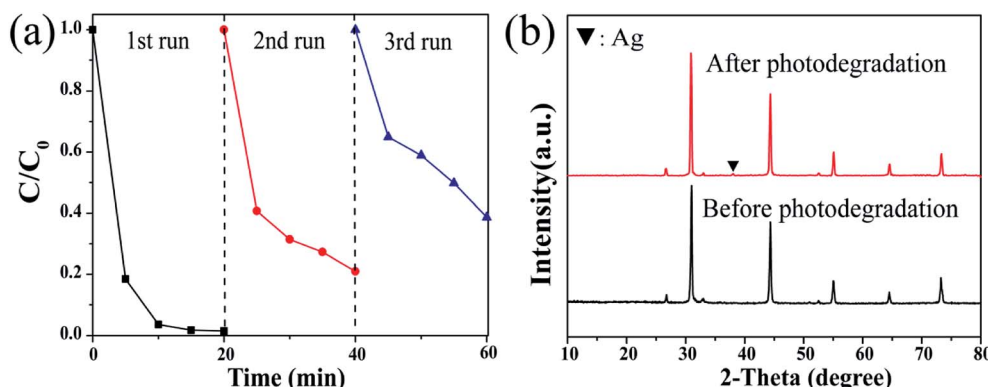


Fig. 9 (a) Reusable performance of S2 and (b) XRD data contrast diagram before and after the use of S2.

To further assess the performance of the photocatalyst, the stability of the photocatalyst was explored through cycling experiments. As shown in Fig. 9a, the catalyst can be subjected to multiple cycling experiments to show that it has good stability; however, after three cycles, the degradation efficiency is reduced, and only 61.3% of the pollutants are degraded. There are two possibilities for explaining this phenomenon: one is that some catalysts are inevitably lost during the experimental operation, and the second is that the catalyst decomposes a part of  $\text{Ag}^0$ ; this directly leads to a decrease in the photocatalytic activity. The latter reason could be supported by the XRD comparison data obtained before and after the sample was used. The  $\text{Ag}^0$  characteristic diffraction peak was clearly observed in the spectrum of the catalyst recovered after the cycling experiment, and the other structures hardly changed (Fig. 9b).

### 3.7. Possible photocatalytic mechanism of the $\text{Ag}/\text{AgBr}/\text{Ag}_3\text{VO}_4$ composites

The photocatalysts produce various active substances in the solution such as hydroxyl radicals ( $\cdot\text{OH}$ ),  $\cdot\text{O}^{2-}$  and  $\text{h}^+$ . The active substances produced can oxidize or reduce the pollutants into new non-toxic and harmless substances; thus, the purpose of removing the target pollutants in the solution is achieved. Therefore, experiments to capture the reactive species have been conducted to identify the active species that are primarily catalytically active. Herein, ammonium oxalate (AO), benzoquinone (BQ) and isopropanol (IPA) acted as scavengers to eliminate  $\text{h}^+$ ,  $\cdot\text{O}^{2-}$  and  $\cdot\text{OH}$ , respectively.<sup>46</sup> As Fig. 10 shows, the degradation rate of MO was 98.6% before the addition of a scavenger, and the removal rate of MO after the addition of AO and BQ was 62% and 21%, respectively. The phenomenon of photocatalytic activity was significantly inhibited; this indicated that  $\text{h}^+$  and  $\cdot\text{O}^{2-}$  might be the main reactive species involved in the photocatalytic degradation process, and  $\cdot\text{O}^{2-}$  played a dominant role in the reaction. When IPA was added as a scavenger, the degradation rate of MO was still as high as 98%, which was enough to show that  $\cdot\text{OH}$  was a partly reactive species in the reaction and had only a weak influence on the degradation process.

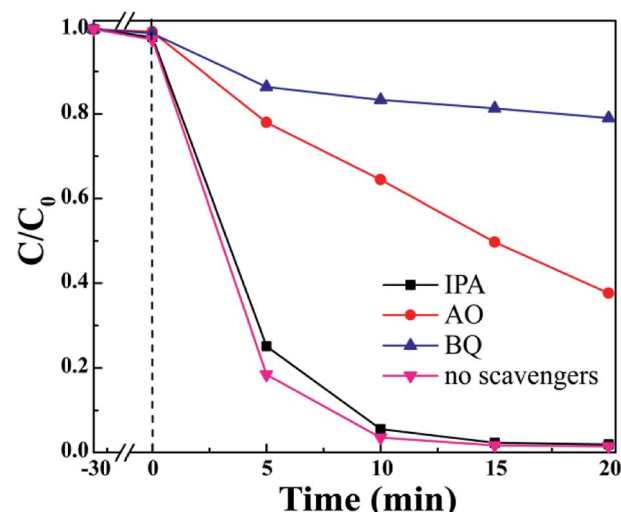


Fig. 10 Photocatalytic degradation of MO in an aqueous solution via S2 under different conditions.

Based on the previous analysis, a possible mechanism for the degradation of MO by the composites can be proposed, as shown in Fig. 11. The band gaps of  $\text{AgBr}$  and  $\text{Ag}_3\text{VO}_4$  estimated by UV-vis spectroscopy were about 2.43 eV and 2.01 eV, respectively. Through the Mulliken electronegativity theory, we computed the position of the semiconductor band, and the formulas are as follows:

$$E_{\text{CB}} = X - E_{\text{e}} - 0.5E_{\text{g}} \quad (1)$$

$$E_{\text{VB}} = E_{\text{CB}} + E_{\text{g}} \quad (2)$$

where  $E_{\text{CB}}$  and  $E_{\text{VB}}$  represent the edge potential of the conduction band (CB) and valence band (VB), respectively, and  $X$  stands for the absolute electronegativity of the semiconductor, which is derived from the geometric mean of the electronegativity of the constituent atoms (the  $X$  value of  $\text{AgBr}$  is 4.42,<sup>47</sup> and the  $X$  value of  $\text{Ag}_3\text{VO}_4$  is 5.64 (ref. 48)).  $E_{\text{e}}$  is the energy of free electrons in the hydrogen scale (about 4.5 eV).  $E_{\text{g}}$  is the band gap energy of the semiconductor. It has been determined by calculation that the valence band edges of  $\text{AgBr}$  and  $\text{Ag}_3\text{VO}_4$  are located at

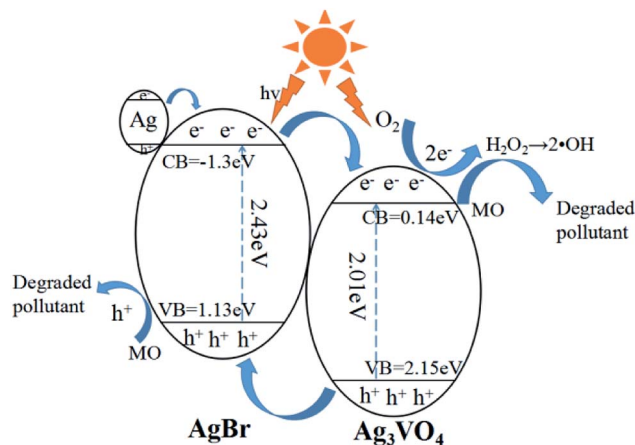
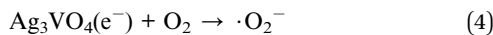


Fig. 11 The possible photocatalytic mechanism of the Ag/AgBr/Ag<sub>3</sub>VO<sub>4</sub> composites.

1.13 eV and 2.15 eV, and the conduction band edges are located at the positions  $-1.3\text{ eV}$  and  $0.14\text{ eV}$ , respectively. Under visible light irradiation, the energy of light is greater than the energy band gap of AgBr and Ag<sub>3</sub>VO<sub>4</sub>. Ag<sup>0</sup>, AgBr and Ag<sub>3</sub>VO<sub>4</sub> can absorb visible light photons to form electron–hole pairs. Subsequently, the electrons will migrate from the surface of Ag<sup>0</sup> to the CB of AgBr and, in turn, eventually to the CB of Ag<sub>3</sub>VO<sub>4</sub>, whereas the holes remain on Ag<sup>0</sup>. The electrons accumulate to a higher concentration in the CB of Ag<sub>3</sub>VO<sub>4</sub>, and the electrons can be trapped by molecular oxygen in the solution to form a strong oxidizing substance,  $\cdot\text{O}_2^-$ , and other reactive oxygen species, which can oxidize MO and result in high photocatalytic activity.<sup>35</sup> Furthermore, the holes in the VB of Ag<sub>3</sub>VO<sub>4</sub> gradually migrate to the VB of AgBr and aggregate. A large number of holes can react with H<sub>2</sub>O or  $\text{--OH}$  to produce the  $\cdot\text{OH}$  radicals, and excess holes can be combined with Br<sup>–</sup> to reduce it to Br<sup>0</sup> since Br<sup>0</sup> is also a kind of active radical species.<sup>35,38,49</sup> Finally,  $\cdot\text{O}_2^-$ , h<sup>+</sup>,  $\cdot\text{OH}$  and Br<sup>0</sup> react with MO as oxidants to generate H<sub>2</sub>O, CO<sub>2</sub> and other small molecules, resulting in the degradation of MO. The possible mechanism by which Ag/AgBr/Ag<sub>3</sub>VO<sub>4</sub> degrades MO can be explained as follows:



On the one hand, the composite material of this structure accelerates the effective separation of photogenerated electrons and holes and reduces the recombination of electron–hole

pairs; on the other hand, Ag<sup>0</sup> on the photocatalyst surface can absorb more visible light, thus further improving the photocatalytic performance.

## 4. Conclusions

A series of Ag/AgBr/Ag<sub>3</sub>VO<sub>4</sub> composites were synthesized by a simple continuous precipitation method. The degradation rates of the sample S2 for MO and TC were 98.6% and 77%, which were better than those of the single photocatalysts Ag<sub>3</sub>VO<sub>4</sub> and Ag/AgBr, indicating that S2 had a better degradation effect on MO and TC in an aqueous solution. In addition, the evidence that h<sup>+</sup> and  $\cdot\text{O}_2^-$  were the main active substances in the degradation process of the pollutant MO was obtained by conducting active group capture experiments. The results of PL, EIS and photocurrent response show that the composite exhibits better charge separation efficiency, and the surface plasmon resonance (SPR) effect of Ag<sup>0</sup> together improves the photocatalytic performance of the composite. As a highly efficient photocatalyst, Ag/AgBr/Ag<sub>3</sub>VO<sub>4</sub> is a promising photocatalyst for wastewater purification.

## Conflicts of interest

The authors declare that they have no conflict of interest.

## Acknowledgements

The authors gratefully acknowledge the financial supports provided by the Guizhou Province High-level Talent Training Program [Talent[2016]5658].

## References

- 1 E. Forgacs, T. Cserháti and G. Oros, *Environ. Int.*, 2004, **30**, 953–971.
- 2 W.-K. Jo and R. J. Tayade, *Chin. J. Catal.*, 2014, **35**, 1781–1792.
- 3 S. Natarajan, H. C. Bajaj and R. J. Tayade, *J. Environ. Sci.*, 2018, **65**, 201–222.
- 4 H. S. Rai, M. S. Bhattacharyya, J. Singh, T. K. Bansal, P. Vats and U. C. Banerjee, *Crit. Rev. Env. Sci. Technol.*, 2005, **35**, 219–238.
- 5 J. Hu, P. Zhang, W. An, L. Liu, Y. Liang and W. Cui, *Appl. Catal., B*, 2019, **245**, 130–142.
- 6 L. Liu, M. Yue, J. Lu, J. Hu, Y. Liang and W. Cui, *Appl. Surf. Sci.*, 2018, **456**, 645–656.
- 7 Y. Zhang, W. Cui, W. An, L. Liu, Y. Liang and Y. Zhu, *Appl. Catal., B*, 2018, **221**, 36–46.
- 8 W. Cui, J. He, H. Wang, J. Hu, L. Liu and Y. Liang, *Appl. Catal., B*, 2018, **232**, 232–245.
- 9 Y. Yang, W. Zhang, R. Liu, J. Cui and C. Deng, *Sep. Purif. Technol.*, 2018, **190**, 278–287.
- 10 J. Kou, C. Lu, J. Wang, Y. Chen, Z. Xu and R. S. Varma, *Chem. Rev.*, 2017, **117**, 1445–1514.
- 11 L. V. Bora and R. K. Mewada, *Renewable Sustainable Energy Rev.*, 2017, **76**, 1393–1421.



12 F. K. Mohamad Alosfur, N. J. Ridha, M. H. H. Jumali and S. Radiman, *Nanotechnology*, 2018, **29**, 145707.

13 M. Hadnadjev-Kostic, T. Vulic and R. Marinkovic-Nedovic, *Adv. Powder Technol.*, 2014, **25**, 1624–1633.

14 V. Moradi, M. B. G. Jun, A. Blackburn and R. A. Herring, *Appl. Surf. Sci.*, 2018, **427**, 791–799.

15 X.-N. Wei, H.-L. Wang, X.-K. Wang and W.-F. Jiang, *Appl. Surf. Sci.*, 2017, **412**, 357–365.

16 C. Mu, Y. Zhang, W. Cui, Y. Liang and Y. Zhu, *Appl. Catal., B*, 2017, **212**, 41–49.

17 G. Wang, X. Ma, B. Huang, H. Cheng, Z. Wang, J. Zhan, X. Qin, X. Zhang and Y. Dai, *J. Mater. Chem.*, 2012, **22**, 21189–21194.

18 L. Liu, L. Ding, Y. Liu, W. An, S. Lin, Y. Liang and W. Cui, *Appl. Catal., B*, 2017, **201**, 92–104.

19 O. Mehraj, N. A. Mir, B. M. Pirzada, S. Sabir and M. Muneer, *J. Mol. Catal. A: Chem.*, 2014, **395**, 16–24.

20 P. Wang, B. Huang, Q. Zhang, X. Zhang, X. Qin, Y. Dai, J. Zhan, J. Yu, H. Liu and Z. Lou, *Chem.-Eur. J.*, 2010, **16**, 10042–10047.

21 Z. Lou, B. Huang, Z. Wang, X. Ma, R. Zhang, X. Zhang, X. Qin, Y. Dai and M.-H. Whangbo, *Chem. Mater.*, 2014, **26**, 3873–3875.

22 J. Liu, W. Wu, Q. Tian, Z. Dai, Z. Wu, X. Xiao and C. Jiang, *Dalton Trans.*, 2016, **45**, 12745–12755.

23 Y. Zhao, L. Kuai and B. Geng, *Catal. Sci. Technol.*, 2012, **2**, 1269–1274.

24 A. Abulizi, K. Kadeer, L. Zhou, Y. Tursun and T. Dilinuer, *J. Taiwan Inst. Chem. Eng.*, 2018, **88**, 243–251.

25 P. Wang, B. Huang, X. Zhang, X. Qin, H. Jin, Y. Dai, Z. Wang, J. Wei, J. Zhan, S. Wang, J. Wang and M. H. Whangbo, *Chem.-Eur. J.*, 2009, **15**, 1821–1824.

26 F. Chen, W. An, L. Liu, Y. Liang and W. Cui, *Appl. Catal., B*, 2017, **217**, 65–80.

27 S. Lin, L. Liu, J. Hu, Y. Liang and W. Cui, *Appl. Surf. Sci.*, 2015, **324**, 20–29.

28 R. Konta, H. Kato, H. Kobayashi and A. Kudo, *Phys. Chem. Chem. Phys.*, 2003, **5**, 3061–3065.

29 Y. Xu, L. Jing, X. Chen, H. Ji, H. Xu, H. Li, H. Li and Q. Zhang, *RSC Adv.*, 2016, **6**, 3600–3607.

30 M. Yan, Y. Wu, F. Zhu, Y. Hua and W. Shi, *Phys. Chem. Chem. Phys.*, 2016, **18**, 3308–3315.

31 M. Yan, Y. Wu, Y. Yan, X. Yan, F. Zhu, Y. Hua and W. Shi, *ACS Sustainable Chem. Eng.*, 2015, **4**, 757–766.

32 F. Kiantazh and A. Habibi-Yangjeh, *Solid State Sci.*, 2015, **49**, 68–77.

33 T. Zhu, Y. Song, H. Ji, Y. Xu, Y. Song, J. Xia, S. Yin, Y. Li, H. Xu, Q. Zhang and H. Li, *Chem. Eng. J.*, 2015, **271**, 96–105.

34 J. Zhang and Z. Ma, *Molecular Catalysis*, 2017, **436**, 190–198.

35 Q. Zhu, W.-S. Wang, L. Lin, G.-Q. Gao, H.-L. Guo, H. Du and A.-W. Xu, *J. Phys. Chem. C*, 2013, **117**, 5894–5900.

36 S. Huang, Y. Xu, Z. Chen, M. Xie, H. Xu, M. He, H. Li and Q. Zhang, *RSC Adv.*, 2015, **5**, 71035–71045.

37 J. Zhang and Z. Ma, *J. Colloid Interface Sci.*, 2018, **524**, 16–24.

38 Z. Wang, J. Zhang, J. Lv, K. Dai and C. Liang, *Appl. Surf. Sci.*, 2017, **396**, 791–798.

39 L. Jing, Y. Xu, C. Qin, J. Liu, S. Huang, M. He, H. Xu and H. Li, *Mater. Res. Bull.*, 2017, **95**, 607–615.

40 M. Gaumet, A. Vargas, R. Gurny and F. Delie, *Eur. J. Pharm. Biopharm.*, 2008, **69**, 1–9.

41 R. Cao, H. Yang, X. Deng, S. Zhang and X. Xu, *Sci. Rep.*, 2017, **7**, 15001.

42 B. Wiley, Y. Sun, B. Mayers and Y. Xia, *Chem. Eur. J.*, 2005, **11**, 454–463.

43 Y. Song, S. Xue, G. Wang, J. Jin, Q. Liang, Z. Li and S. Xu, *J. Phys. Chem. Solids*, 2018, **121**, 329–338.

44 T. Li, Y. He, H. Lin, J. Cai, L. Dong, X. Wang, M. Luo, L. Zhao, X. Yi and W. Weng, *Appl. Catal., B*, 2013, **138–139**, 95–103.

45 S. Zhang, H. Gao, X. Liu, Y. Huang, X. Xu, N. S. Alharbi, T. Hayat and J. Li, *ACS Appl. Mater. Interfaces*, 2016, **8**, 35138–35149.

46 J. Zhang and Z. Ma, *J. Taiwan Inst. Chem. Eng.*, 2018, **88**, 177–185.

47 K. Dai, D. Li, L. Lu, Q. Liu, C. Liang, J. Lv and G. Zhu, *Appl. Surf. Sci.*, 2014, **314**, 864–871.

48 S. Wang, D. Li, C. Sun, S. Yang, Y. Guan and H. He, *Appl. Catal., B*, 2014, **144**, 885–892.

49 Y. Wan, C. Liang, Y. Xia, W. Huang and Z. Li, *Appl. Surf. Sci.*, 2017, **396**, 48–57.

